Inverse-photoemission study of Ge(100), Si(100), and GaAs(100): Bulk bands and surface states

J. E. Ortega and F. J. Himpsel
IBM Thomas J. Watson Research Center, P.O. Box 218, New York, New York 10598
(Received 14 July 1992)

We present momentum-resolved inverse-photoemission data from Ge(100)2×1, Si(100)2×1, and GaAs(100)4×2 surfaces. The bulk conduction bands of these three semiconductors are mapped along the ΓX direction. The following critical points are obtained (relative to the valence-band maximum): For Ge, $L_{3c}=4.4$ eV and $L'_{2c}=7.8$ eV; for Si, $\Gamma_{15c}=3.05$ eV, $\Gamma'_{2c}=4.1$ eV, and $X_{1c}=1.25$ eV; for GaAs, $L_{3c}=5.45$ eV and $L_{1c}=8.6$ eV. The L points are reached via surface umklapp processes. The experimental band dispersions and the critical points are consistent with state-of-the-art quasiparticle calculations. The empty π^* surface state is seen in Si and Ge. Its cross section changes significantly with the photon energy, reflecting a wave-function character derived from that of the bulk states near Γ.

I. INTRODUCTION

The band theory of semiconductors has been expanded in recent years to include self-energy effects.[1–5] These effects mainly influence the band gap but also have an influence on band dispersions. In the last few years, the filled bands and many of the empty bands of the common semiconductors (Ge, Si, GaAs) have been mapped with photoemission and inverse-photoemission measurements.[6–8] There is still a piece missing, i.e., the empty bands along the ΓX line. In order to complete the experimental information, we performed momentum-resolved, energy-dependent inverse-photoemission measurements on the (100) surfaces of Ge, Si, and GaAs.

Due to its technological importance, the Si(100) surface has been extensively studied from both the theoretical and experimental points of view.[8] Ideally, the truncation of the bulk produces a (100) surface with two dangling bonds per silicon surface atom. As is widely accepted, adjacent silicon surface atoms pair up in the 2×1 reconstruction, forming asymmetric dimers that reduce the number of dangling bonds to one per surface atom. The asymmetry is required to explain the semiconducting character of the surface,[9] and the stable, low-temperature $c(4\times2)$ reconstruction.[10] The same description of the surface holds for Ge(100). The two dangling bonds in the dimer interact weakly and form localized π bonding and π^* antibonding states. In a band picture the terms π-like filled surface band and π^*-like empty surface band are used. Both have been mapped along high-symmetry directions using photoemission.[11] For this purpose, highly n-doped samples are used to populate the π^* empty surface state.[12] The wave-function character of these surface states is revealed from the photon energy dependence of their photoemission intensity.[13] Here we analyze the photon energy dependence of the inverse-photoemission intensity from Si(100)2×1 and extend the same analysis to the case of Ge(100).

II. EXPERIMENT

Our inverse-photoemission spectrometer uses a fast $f/4$ grating monochromator with simultaneous detection of photons with energies between 8 and 20 eV.[14] A parallel electron beam from a Pierce-type electron gun with a low-temperature BaO cathode impinges onto the sample surface. Photons are detected at 45° from the surface normal; consequently the electric-field component **E** parallel to the surface has a three-times higher detection probability than the perpendicular component. Energy and momentum resolution of 0.27 eV and 0.1 Å^{-1}, respectively, can be achieved with this instrument. The energy $h\nu$ of the emitted photon is measured for a chosen initial electron energy E_i; the latter being referred to the sample Fermi level E_F. In the spectra discussed in the next sections, the photon energies have been converted into final-state energies according to $E_F=E_i-h\nu$. The reference energy for the spectra and for the data points in the $E(k)$ plots is the valence-band maximum (VBM). In order to get the value (E_F-VBM), an independent measurement of the Fermi level inside the gap is required. We use 0.1, 0.45, and 0.75 eV above the VBM for p-Ge(100),[15] n-Si(100),[16] and p-GaAs(100),[17] respectively.

Clean Ge(100) surfaces were prepared by sputter annealing well-oriented (0.4°) wafers (p doped). The final annealing temperature was 500 °C. The Si(100) clean surfaces (n doped) were obtained by the standard procedure of short flashing to 1050 °C, followed by slow cooling down from 850 °C with the pressure always below 10^{-9} Torr. In the three cases, strong emission from the surface-related features, especially surface states, assured the quality of the surfaces. In order to prevent contamination, the surface reconstruction was checked with low-energy electron diffraction (LEED) after the measurements. Si(100) displayed low-background, sharp 2×1 LEED pattern. Ge(100) showed a sharp 2×1 LEED pattern with traces of $c(2\times4)$. GaAs(100) surfaces were obtained by soft Ar^+ sputtering (500 eV) and

 ©1993 The American Physical Society

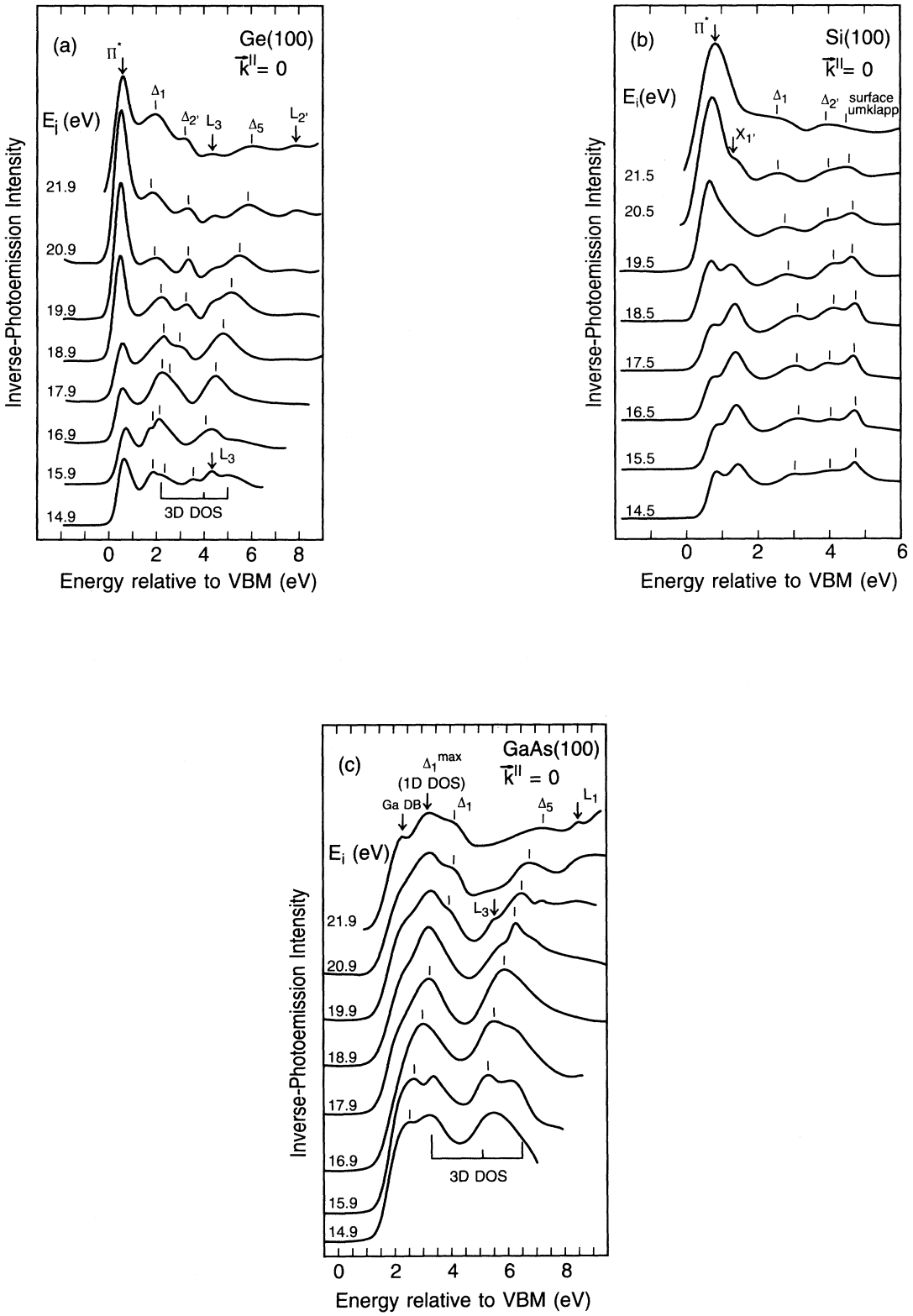

FIG. 1. Normal incidence inverse-photoemission spectra from (a) Ge(100)2×1, (b) Si(100)2×1, and (c) GaAs(100)4×2. The energy of the incident electrons is being referred to the Fermi level. Dispersive features are marked with ticks and correspond to transitions between bulk bands. The remaining peaks are assigned to empty surface states (π^* for Si and Ge, and Ga dangling bond for GaAs), surface umklapp (to the L point), and to 1D DOS. The position and the relative intensity of the main peaks in the BIS spectra of Ref. 20 are also indicated in the cases of Ge and GaAs.

annealing (550 °C) cycles on p-doped wafers ($10^{18}\times$ cm^{-3}). The LEED pattern from these surfaces showed a sharp, low-background 4×2 reconstruction with traces of 4×6 reconstruction and corresponds to that of a well-ordered Ga-rich surface.[18]

III. INVERSE-PHOTOEMISSION RESULTS AND ASSIGNMENT OF TRANSITIONS

Inverse-photoemission spectra from Ge(100)2×1, GaAs(100)4×2, and Si(100)2×1 surfaces are shown in Figs. 1(a)–1(c). The data are analyzed in terms of surface and bulk interband transitions. The ticks mark the position of the peaks that show appreciable dispersion with changing initial energy, whereas the arrows indicate nondispersive transitions. As mentioned in the preceding section, the incident-energy values are relative to the Fermi level, while binding energies are referred to the VBM. Very useful information is also provided by the E_i dependence of the photoemission intensity from the different transitions, especially in the case of nondispersing peaks. For this purpose, the spectra of Fig. 1 have been normalized to the deposited charge. Additionally, we will try to be consistent in the assignment of the features, i.e., we will look for the same transitions in the three surfaces, especially in the cases of Ge and GaAs, since they have similar band topology. Four different assignments of the peaks have to be considered, i.e., vertical transitions between bulk bands, contributions from the one- and three-dimensional density of states (1D DOS and 3D DOS, respectively), and surface effects (surface states and surface umklapp processes). The spectra of Fig. 1 will be discussed in terms of these phenomena.

A. Direct transitions between bulk bands

As depicted in Fig. 2, with the incident electrons normal ($\mathbf{k}^{\parallel}=\mathbf{0}$) to the (100) surfaces of Ge, Si, and GaAs, interband transitions take place along the ΓX line in the Brillouin zone. The assignment of the peaks to the different transitions is better understood in the light of the calculated bulk band structure, such as the one displayed in Fig. 3. In the left part of this figure, the result of an empirical pseudopotential calculation for the bulk band structure of Ge along the ΓX line is presented.[19] The energies are referred to the VBM and the point symmetry of each band is indicated. A very similar band topology is obtained in the case of GaAs and Si.[20]

For direct transitions between bulk states, the initial energy of the electron E_i can be converted directly into the momentum $\mathbf{k}^{\perp}$ using the $E(\mathbf{k}^{\perp})$ relation of an upper band in Fig. 3. The probability of populating an initial band goes down the farther the direction of its principal lattice vector deviates from the momentum of the incident electron. Therefore one first tries the "primary cone" as upper initial-state band, i.e., a free-electron-like band shifted down by an inner potential V_0 and backfolded into the first Brillouin zone by reciprocal-lattice vectors perpendicular to the surface. The dashed line in Fig. 3 is the primary cone for Ge using $V_0=-8.8$ eV with respect to the VBM. This value for the inner potential is obtained by matching, at the center of the ΓX line, the free-electron parabola to the final photoemission band of Ref. 21. Along ΓX, the real band closest to this primary cone is Δ_2'. The upper part of this band is in very good agreement with the photoemission experiments of Nelson *et al.*[21] In this work, we will use the calculated bands from Ref. 19 as our initial-state upper bands for Ge, whereas for Si and GaAs we have taken the upper bands from Ref. 20. We can also adjust the free-electron para-

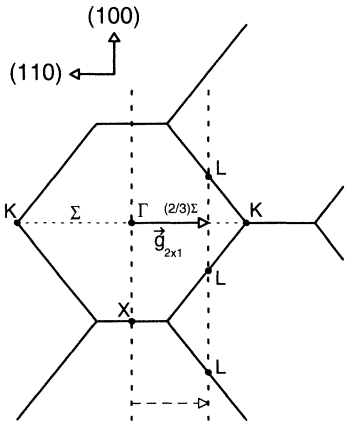

FIG. 2. Side view of the bulk Brillouin zone for the diamond lattice. With the incident electrons normal to the (100) surface, bulk transitions take place along the ΓX line. In addition, the line between L and $\frac{2}{3}\Sigma$ point can be reached with a $\mathbf{g}_{2\times1}$ surface umklapp process.

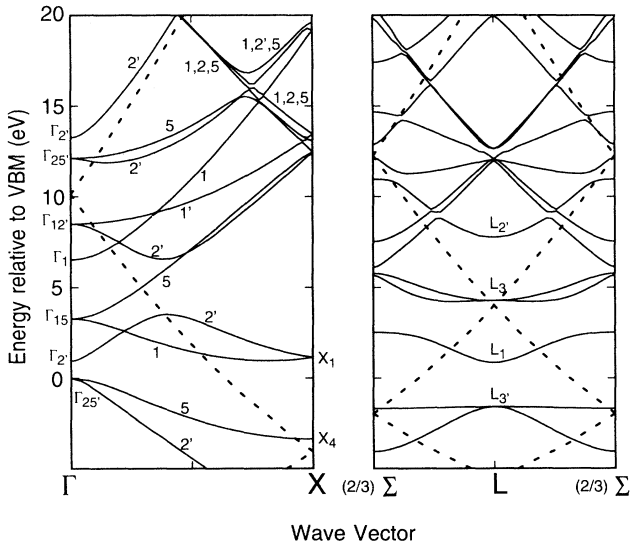

FIG. 3. Band structure of Ge calculated with the pseudopotential model and parameters of Ref. 19 along the ΓX line (left panel) and the $\frac{2}{3}\Sigma L$ line (right panel). The latter is accessible in normal incidence via surface umklapp, as shown in Fig. 2. The dashed lines represent the free-electron-like bands calculated with the inner potential $V_0=-8.8$ eV.

bola to the upper Δ_2' bands in Ref. 20 to obtain the inner potential for Si ($V_0=-9.0$ eV) and GaAs ($V_0=-9.0$ eV).

In the inverse-photoemission spectra from Ge(100) in Fig. 1(a), the dispersing peaks are assigned to vertical transitions from the primary cone, i.e., transitions from the upper Δ_2' to the three lower conduction bands Δ_2', Δ_1, and Δ_5. The $\Delta_2'\rightarrow\Delta_1$ transition disperses from 2.4 down to 1.95 eV, while the $\Delta_2'\rightarrow\Delta_2'$ goes through an extreme point at 3.4 eV with $E_i=19.9$ eV. At this extreme point the density of states is higher and a maximum in the intensity is observed. The peak attributed to the $\Delta_2'\rightarrow\Delta_5$ transition disperses steadily upwards from 3.5 to 6.1 eV.

The spectra for Si(100) are presented in Fig. 1(b). There is a dispersive feature that shifts from 3.0 to 2.5 eV with increasing E_i, and is assigned to the $\Delta_2'\rightarrow\Delta_5$ transition. The peak around 4 eV exhibits a turning point at $E_i=17.5$ eV, where the photoemission intensity is also maximum. This peak is assigned to the bulk transition from the primary cone to the conduction band Δ_2'. Another peak shows slight downward dispersion in the Si(100) spectra. This peak is assigned to the transition from the high-lying Δ_1 band to the Δ_1 band (in the conduction-band region) down to the X_{1c} point, which is found at 1.25 eV. This transition involves the bulk reciprocal vector $\mathbf{G}=(111)$. In the energy region examined here, the Δ_1 band is almost flat, which explains the small dispersion.

The inverse-photoemission (IPE) spectra of GaAs(100) presented in Fig. 1(c) are similar to those of Ge(100), especially at higher incident energies. Such similarity is expected from their band topology. This is especially helpful for the assignments in the low-energy part of the IPE spectra in Fig. 1(c), where different transitions overlap. For this reason, the intensity of the peaks has not been analyzed. In GaAs the symmetry is lowered with respect to Si or Ge and the bands along Δ have only two different point symmetries, i.e., Δ_1 and Δ_5. The tick marks indicate the best estimate for the bulk transitions. With increasing incident energy, the $\Delta_1\rightarrow\Delta_1$ transition disperses from 2.6 to 4.15 eV, and the $\Delta_1\rightarrow\Delta_5$ disperses from 5.3 to 7.2 eV.

B. Symmetry and selection rules

The bulk bands of the diamond structure have two symmetries with nonvanishing amplitude along the [100] direction,[22] i.e., Δ_1 and Δ_2'. Note that these Δ symmetry representations are not the same as for the fcc structure, despite identical symbols. The diamond structure has combined translations-rotations along the [100] direction, while the fcc structure does not have translations. As a consequence, there is only one symmetry with nonvanishing amplitude along [100] for the fcc lattice, i.e., Δ_1. An additional complication to be considered is the lowering of the symmetry along the Δ axis when the bulk diamond structure is truncated at the (100) surface. All symmetry operations involving translations along the [100] direction are lost after truncation and the symmetry is lowered from fourfold to twofold. This is similar to the lowering of the symmetry from sixfold to threefold at the (0001) surface of the hcp lattice.[23] The selection rules for dipole transitions along the Δ axis are such that all transitions are allowed. These can be derived using established methods for nonsymmorphic space groups.[24,25] At the X point one has the allowed transitions $X_1\rightarrow X_1$, $X_2\rightarrow X_2$, and $X_3\rightarrow X_4$ for the electric-field vector $\mathbf{A}$ along the $\Gamma\Delta X$ direction, and $X_1, X_2\rightarrow X_3, X_4$ for $\mathbf{A}$ perpendicular to $\Gamma\Delta X$. The selection rules at Γ are the same as for fcc and bcc lattices, which are tabulated in Ref. 26. In the zinc-blende structure the symmetry is lowered, thereby making symmetry selection rules even less stringent than for diamond.

C. One- and three-dimensional density of states

Transitions from the primary cone generally dominate, but there is experimental evidence for contributions from other bands, specially in III-V compounds.[27] In addition, one can have evanescent initial states that do not conserve $\mathbf{k}^{\perp}$. In such cases, with normal incidence on (100) surfaces, one is probing many $\mathbf{k}$ points along ΓX, and thus obtaining an averaged spectrum. The average reflects the one-dimensional density of states along ΓX. This is the situation for the peak at 3.35 eV in the GaAs(100) spectra, which we assign to the 1D density of states along ΓX for the Δ_1 band.

Additionally, at lower incident energies the incoming electron wave can be strongly perturbed by steps and defects and momentum conservation is lost completely. Many parts of the Brillouin zone can contribute to the spectrum, resulting in three-dimensional DOS effects. This kind of emission has been observed with low E_i on poorly cleaved GaAs(110).[27] Similar 3D-DOS effects have been reported for photoemission.[28] The peak at 5.0 eV in the spectra of Ge(100) (more intense with $E_i=14.9$ eV) and the peak at 6.25 eV in the GaAs(100) spectra ($E_i=14.9-16.9$ eV) belong to this category. These energies compare well with the features of the integrated bremsstrahlung isochromat (BIS) spectra observed at 5.0 eV in Ge(100) and at 6.5 eV in GaAs(100).[20] The position and the relative intensity of the main peaks in the BIS spectra of Ref. 20 are indicated at the bottom of Figs. 1(a) and 1(c). The structures at 4.4 and 3.35 eV in the spectra of Ge(100) and GaAs(100) [Figs. 1(a) and 1(c), respectively], appear around the same energy region as the strongest peaks of the BIS spectra for Ge (4.0 eV) and GaAs (3.3 eV).[20] Therefore, we cannot rule out the possibility that significant emission from the mentioned features, specially at low E_i, is due to 3D-DOS effects.

D. Surface umklapp and surface states

With the 2×1 surface reconstruction in Si(100) and Ge(100), one has to take into account the possibility of a surface umklapp, i.e., the addition of a half-order reciprocal-lattice vector $\mathbf{g}_{2\times1}$ of the surface to the momentum balance. That makes another line in the bulk Brillouin zone accessible with normal incidence. As can be seen in Fig. 2, this line passes through L and crosses the Σ line at $\frac{2}{3}(2\pi/a)$ Å^{-1} from the center of the zone. In the right-hand part of Fig. 3 we plot the energy bands

obtained from the pseudopotential calculation of Ref. 19 along this line [the $(\frac{2}{3})\Sigma L$ line]. In the case of the Ga-rich GaAs(100)4×2 surface, the Ga atoms pair and form dimers along the $[1\bar{1}0]$ direction, leading to a twofold periodicity.[18] Therefore, we have the same $\mathbf{g}_{2\times1}$ surface lattice vector along $[1\bar{1}0]$, and the process shown in Fig. 2 may occur.

The dashed lines in the right panel of Fig. 3 represent the free-electron-like band calculated with the inner potential $V_0=-8.8$ eV. The upper branch of this band is close to our inverse-photoemission initial state. This initial-state band crosses the L point at $E=20.0$ eV, which is within our incident-energy range. Since the inner potential and the lattice constant are almost the same for GaAs, we expect a similar value for the crossing point of the upper band at L. For Si we obtained the same inner potential as for GaAs, but the Brillouin zone is larger. Therefore the upper initial state will lie higher in energy compared to the same band in GaAs or Ge. In Si the upper branch of the primary cone (calculated with $V_0=-9.0$) goes from $E=14.1$ eV at $(\frac{2}{3})\Sigma$ to $E=25.7$ eV at L, whereas in Ge the same part of the band goes from $E=12.5$ eV at $(\frac{2}{3})\Sigma$ to $E=23.1$ eV at L. Consequently for Si, within our photon energy range and with a surface umklapp process involved, we are looking at the center of the $(\frac{2}{3})\Sigma L$ line.

Surface umklapp features appear in the spectra of Ge, Si, and GaAs, see Fig. 1. Transitions to the L_{3c} and L'_{2c} points lead to the nondispersive peaks that show up at higher E_i in the spectra from Ge (L_{3c} at 4.4 eV and L'_{2c} at 7.8 eV) and from GaAs (L_{3c} at 5.45 eV and L'_{2c} at 8.6 eV). The results for Ge are in good agreement with the values obtained in inverse-photoemission experiments from Ge(111) (L_{3c} at 4.2 eV and L'_{2c} at 7.9 eV).[29] The intensity of the L'_{2c} peak is maximum $E_i=20.9$ in both Ge and GaAs. The maxima occur when the primary cone-related upper band crosses L (at 20.0 eV in Fig. 3) and direct vertical transitions to the high density of states at L'_{2c} or L_{3c} are possible. The intensity analysis cannot be performed for the L_{3c} point in Ge or GaAs due to the overlap with the $\Delta'_2\rightarrow\Delta_5$ peak. The peak that shifts from 4.75 eV (at $E_i=14.5$ eV) to 4.5 eV ($E_i=21.5$ eV) in the spectra of Si [Fig. 1(b)] corresponds to a transition to the band that disperses down to L_{3c} (see Fig. 3). The value of 4.5 eV is far from the L_{3c} point found at 4.15 eV in inverse-photoemission experiments on Si(111).[29] This result is expected since the primary cone-related upper band in Si crosses L at higher energy than in Ge and is out of our initial energy range.

Surface states are identified by the lack of $\mathbf{k}^{\perp}$ dispersion and by the sensitivity to adsorbates. The large features closest to the band gap in Fig. 1 are assigned to transitions to the empty surface states. In Ge and Si the surface state is the π^* dangling bond, found at 0.60 and 0.72 eV above the VBM, respectively. In GaAs a surface state appears at 2.40 eV above the VBM, and it corresponds to the Ga empty dangling bond. The adsorbate sensitivity test of the surface features is presented in Fig. 4, where we compare the spectra taken from freshly prepared surfaces with the spectra of surfaces contaminated upon pro-

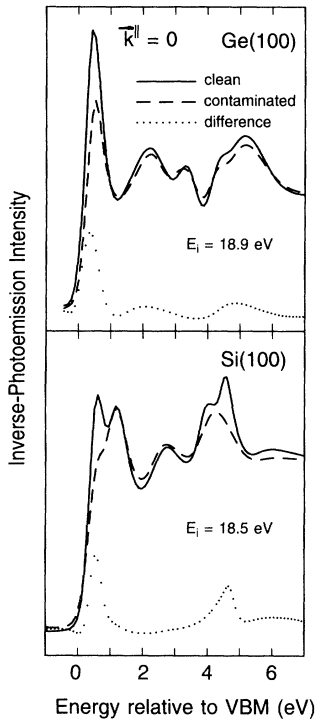

FIG. 4. Inverse-photoemission spectra of Ge(100) (top panel) and Si(100) (bottom panel) for clean 2×1 surfaces (solid lines) and after being contaminated (dashed lines). The difference spectra are shown in dotted lines. The peaks associated with the surface states are strongly affected by the contamination, as well as the surface umklapp peak in Si.

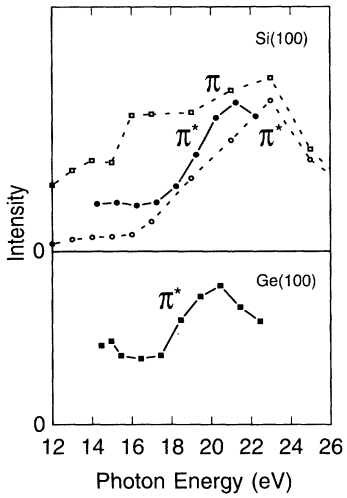

FIG. 5. Photon-energy dependence of the π^* surface state in Si and Ge (full symbols and lines). The result is compared with a similar intensity analysis of the π and π^* dangling bonds (open symbols and dashed lines) in direct photoemission spectra (Ref. 13). The resonance appears for initial states near Γ, showing that the surface states are derived from bulk bands in Γ.

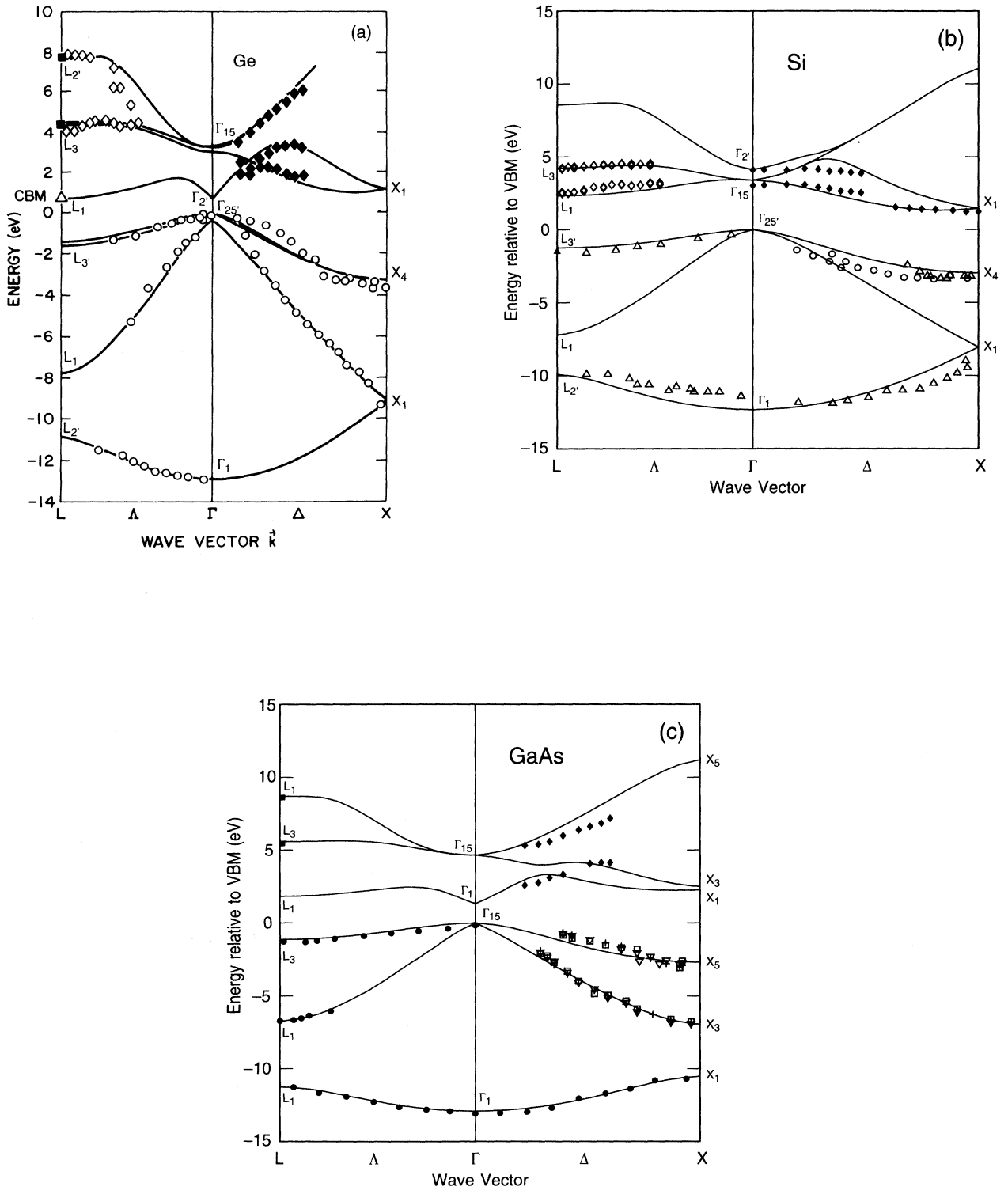

FIG. 6. Energy-band dispersions for (a) Ge, (b) Si, and (c) GaAs along $L\Gamma X$ from inverse-photoemission and photoemission: full diamonds and full squares, this work; open diamonds, data taken from Ge(111)2×1 and Si(111)2×1 (Ref. 29); circles, from Si(100)2×1 (Ref. 35); open triangles, from Sb-saturated Si(100) and Si(111) (Ref. 36); open squares, open dels and crosses from GaAs(100)1×1, GaAs(100)$c(2\times8)$, and GaAs(100)$c(6\times4)$, respectively (Ref. 37); filled circles, from GaAs(110) (off-normal) (Ref. 38); full triangle from Si(111)2×1 (Ref. 33). The solid lines represent the results from a first-principles quasiparticle calculation by Hybertsen and Louie [for Ge (Ref. 1)] and by Zhu and Louie [for Si and GaAs (Ref. 4)]. The observed differences are within the experimental and theoretical errors.

longed exposure to the residual gas in the chamber. The difference spectra are presented in the same figure. The surface states in both cases are strongly affected by the contamination, as is the transition to L_{3c} via surface umklapp in Si. Here we notice that the same transition in Ge remains almost unaffected. Generally, the Ge(100) surface is found to be less reactive than Si(100). We can also have, at 0.60 eV, contributions from a surface umklapp to L_{1c} as in Ref. 29. This contribution would remain in the spectrum from the contaminated surface, since our type of contamination does not alter the 2×1 reconstruction in Ge(100). For GaAs, all the surface features become more intense when improving the surface preparation.[30]

The intensity of the π^* peaks of both Si and Ge changes dramatically as a function of E_i, showing a clear maximum for incident energies of 21.5 and 21.9 eV for Si and Ge, respectively. In Fig. 5, the intensity of the surface states of Si and Ge is plotted as a function of the photon energy. The dashed lines in Fig. 5 correspond to the same intensity analysis performed in photoemission experiments on Si for both the π and the π^* dangling bonds[13] (the π^* surface state can be populated by using highly doped n-type samples, and hence be measured in direct-photoemission experiments). The photoemission data of Fig. 5 have been normalized to the inverse-photoemission data in the same figure and corrected with the energy-dependent phase-space factor $(h\nu)^2/E_{\rm kin}$.[31] Within the experimental error, the intensity maxima for the π^* peak in Si coincide. The energy position of these maxima allows conclusions about the wave-function character of the surface states.[32] In general, surface states split off from bulk bands at critical points. Transitions between surface states and bulk states with a wave vector similar to that of the critical point nearest to the surface state will be enhanced. The intensity maxima appearing in our case at $h\nu=22\pm1$ eV for both Si and Ge could either correspond to transitions from the L'_{25c} point of a secondary cone,[13] or to the surface umklapp of the L point of the primary cone (Fig. 3, dashed lines). On the Si(111)2×1 surface, an intensity maximum has been seen for the π surface state at the same L point.[33] Notice that the π^* states are rather weak at a photon energy of 9.7 eV, where fixed photon energy detectors operate.[34]

IV. EXPERIMENTAL BAND DISPERSIONS AND COMPARISON WITH FIRST-PRINCIPLES THEORY

The energies of the different peaks of Fig. 1 are plotted as functions of $\mathbf{k}^{\perp}$ in Fig. 6. To convert our incident energies into $\mathbf{k}^{\perp}$, we use the band-structure calculation of Ref. 19 for Ge, and those of Ref. 20 for Si and GaAs. The portion of the primary cone used here corresponds to the upper Δ'_2 band of Fig. 3. For the secondary cone transition observed in Si, the initial state is the Δ_1 coming from the Γ_1 at ~8.5 eV.[20] In order to compare our experimental data with theoretical band structures, we have included in Fig. 6 the results of recent quasiparticle energy calculations for Ge,[1] Si, and GaAs,[4] which represent the state of the art in band theory. In the quasiparticle description of the energy bands one actually calculates the excited state, which is measured either in photoemission (final positive ion state) or inverse-photoemission (final negative ion state). Traditional calculations provide only energy eigenvalues for the ground state, which can not be verified experimentally. The quasiparticle results for Ge are presented in Fig. 6(a). The full diamonds represent the experimental data obtained in this work. We have also included photoemission and inverse-photoemission data from Refs. 35 and 29, respectively. The agreement with the quasiparticle calculation is excellent. The critical points at L, i.e., L_{3c} (4.4 eV) and L'_{2c} (7.8 eV) also match with the calculated values (4.4 and 7.7 eV, respectively).

Our results for Si are presented in Fig. 6(b) as full diamonds. Additional photoemission and inverse-photoemission data are from Refs. 35, 36, and 29, respectively. The Δ_1 band is well reproduced by the calculation. The measured Δ'_2 band does not appreciably disperse. Here two different phenomena may reduce the observed dispersion: emission from the nearby Δ_5 band and 1D-DOS or 3D-DOS contributions that show up strongly in the BIS spectra.[20] The numerical values (in eV) for the critical points of Si obtained in this work and compared with the calculated ones[4] are $\Gamma_{15c}=3.05$ eV (3.43 eV in the calculation), $\Gamma'_{2c}=4.1$ eV (4.23 eV), and $X_{1c}=1.25$ eV (1.47 eV). The critical points in the calculation lie higher in energy by 0.2 eV.

For GaAs the results are shown in Fig. 6(c). The experimental photoemission data are taken from Refs. 37 and 38. We observe that the calculated Δ_5 band disperses more than the measured one, while Δ_1 agrees reasonably well. Here we notice that the Δ_5 band along ΓX disperses upwards much faster than any other band coming from Γ_{15c}. Therefore, the finite angular distribution of the electron beam around the surface normal tends to lower the energy at a given $\mathbf{k}^{\perp}$.[39] The experimental values for L_{3c} (5.45 eV) and L_{1c} (8.6 eV) are in agreement with the calculated ones (at 5.4 and 8.3 eV, respectively). The deviation observed for L_{1c} is within the experimental and theoretical error.

ACKNOWLEDGMENTS

We express our gratitude to P. Kirchner for etching the GaAs wafers and to W. Grobman for providing us with a pseudopotential band-calculation program. We also acknowledge X. Zhu and S. Louie for allowing us to use their unpublished quasiparticle calculations.

[1] M. S. Hybertsen and S. G. Louie, Phys. Rev. B **34**, 5390 (1986); and S. G. Louie (private communication).

[2] W. von der Linden and P. Horsch, Phys. Rev. B **37**, 8351 (1988).

[3] R. W. Godby, M. Schlüter, and L. J. Sham, Phys. Rev. B **37**, 10 159 (1988).

[4] X. Zhu and S. G. Louie, Phys. Rev. B **43**, 14 142 (1991); and (private communication).

[5]R. Hott, Phys. Rev. B **44**, 1057 (1991).
[6]T. C. Chiang and F. J. Himpsel, in *Electronic Structure of Solids: Photoemission Spectra and Related Data,* edited by A. Goldman and E.-E. Koch, Landolt-Börnstein, New Series, Group III, Vol. 23a (Springer-Verlag, Berlin, 1989), p. 103.
[7]F. J. Himpsel, Surf. Sci. Rep. **12**, 1 (1990).
[8]G. V. Hansson and R. I. G. Uhrberg, Surf. Sci. Rep. **9**, 197 (1988), and references therein.
[9]F. J. Himpsel and D. E. Eastman, J. Vac. Sci. Technol. **16**, 1297 (1979).
[10]Y. Enta, S. Suzuki, and S. Kono, Phys. Rev. Lett. **65**, 2704 (1990); R. A. Wolkow, *ibid.* **68**, 2636 (1992).
[11]L. S. O. Johansson, R. I. G. Uhrberg, P. Mårtensson, and G. V. Hansson, Phys. Rev. B **42**, 1305 (1990).
[12]P. Mårtensson, A. Cricenti, and G. V. Hansson, Phys. Rev. B **33**, 8855 (1986).
[13]L. S. O. Johansson, E. Landemark, G. V. Hansson, and R. I. G. Uhrberg, Surf. Sci. **211/212**, 578 (1989).
[14]Th. Fauster, D. Straub, J. J. Donelon, D. Grimm, A. Marx, and F. J. Himpsel, Rev. Sci. Instrum. **56**, 1212 (1985).
[15]T. Miller, E. Rosenwinkel, and T. C. Chiang, Phys. Rev. B **30**, 570 (1984).
[16]F. J. Himpsel, B. S. Meyerson, F. R. McFeely, J. F. Morar, A. Taleb-Ibrahimi, and J. A. Yarmoff, in *Photoemission and Absorption Spectroscopy of Solids and Interfaces with Synchrotron Radiation,* Proceedings of the Enrico Fermi School, edited by M. Campagna and R. Rosei (North Holland, Amsterdam, 1990), p. 203.
[17]X. Yin, H. M. Chen, F. H. Pollack, Y. Chan, P. A. Montano, P. D. Kirchner, G. D. Pettit, and J. M. Woodall, J. Vac. Sci. Technol. A **10**, 131 (1992).
[18]M. D. Pashley, K. W. Haberern, W. Friday, J. M. Woodall, and P. D. Kirchner, Phys. Rev. Lett. **60**, 2176 (1988).
[19]W. D. Grobman, D. E. Eastman, and J. L. Freeouf, Phys. Rev. B **12**, 4405 (1975).
[20]J. R. Chelikowsky, T. J. Wagener, J. H. Weaver, and A. Jin, Phys. Rev. B **40**, 9644 (1989).
[21]J. G. Nelson, W. J. Gignac, R. S. Williams, S. W. Robey, J. G. Tobin, and D. A. Shirley, Surf. Sci. **131**, 290 (1983).
[22]L. S. O. Johansson, P. E. S. Persson, U. O. Karlsson, and R. I. G. Uhrberg, Phys. Rev. B **42**, 8991 (1990).
[23]F. J. Himpsel and D. E. Eastman, Phys. Rev. B **20**, 3217 (1979); **21**, 3207 (1980).
[24]M. Lax and J. J. Hopfield, Phys. Rev. **124**, 115 (1961).
[25]R. J. Elliot and R. Loudon, J. Phys. Chem. Solids **15**, 146 (1960).
[26]W. Eberhardt and F. J. Himpsel, Phys. Rev. B **21**, 5572 (1980); **23**, 5650 (1981).
[27]D. Straub, M. Skibowski, and F. J. Himpsel, Phys. Rev. B **32**, 5237 (1985).
[28]F. Cerrina, J. R. Myron, and G. J. Lapeyre, Phys. Rev. B **29**, 1798 (1984).
[29]D. Straub, L. Ley, and F. J. Himpsel, Phys. Rev. B **33**, 2607 (1986).
[30]M. Gallagher, G. J. Mankey, R. F. Willis, J. E. Ortega, and F. J. Himpsel (unpublished).
[31]F. J. Himpsel, Phys. Scr. **T31**, 171 (1990).
[32]S. G. Louie, P. Thiry, R. Pinchaux, Y. Petroff, D. Chandesris, and I. Lecante, Phys. Rev. Lett. **44**, 549 (1980).
[33]F. J. Himpsel, P. Heimann, and D. E. Eastman, Phys. Rev. B **24**, 2003 (1981).
[34]L. S. O. Johansson and B. Reihl, Phys. Rev. Lett. **67**, 2191 (1991); L. S. O. Johansson and B. Reihl, Appl. Surf. Sci. **56-58**, 486 (1992).
[35]A. L. Wachs, T. Miller, T. C. Hsieh, A. P. Shapiro, and T. C. Chiang, Phys. Rev. B **32**, 2326 (1985).
[36]D. H. Rich, T. Miller, G. E. Franklin, and T. C. Chiang, Phys. Rev. B **39**, 1438 (1989).
[37]T. C. Chiang, R. Ludeke, M. Aono, G. Landgren, F. J. Himpsel, and D. E. Eastman, Phys. Rev. B **27**, 4770 (1983).
[38]T. C. Chiang, J. A. Knapp, M. Aono, and D. E. Eastman, Phys. Rev. B **21**, 3513 (1980).
[39]One can improve the agreement with the pseudopotential calculation by using a free-electron-like initial state with a convenient inner potential. However, we have tried to be consistent with the initial state used in Ge and Si, as well as with the direct-photoemission data plotted in Fig. 6(c): the band used in this work lies between the free-electron-like parabolas of Ref. 37 ($V_0 = -7.7$ eV) and Ref. 38 ($V_0 = -9.34$ eV).